Optical properties of periodic structures of metallic nanodisks

G. Gantzounis and N. Stefanou
Section of Solid State Physics, University of Athens, Panepistimioupolis, GR-157 84 Athens, Greece

N. Papanikolaou
Institute of Microelectronics, NCSR "Demokritos," GR-153 10 Athens, Greece

(Received 26 October 2007; published 2 January 2008)

Plasmonic systems of two- and three-dimensional ordered arrays of metallic nanodisks are studied by means of full-electrodynamic calculations using the layer-multiple-scattering method. In particular, we investigate the electromagnetic interaction of waveguide modes of an indium tin oxide film on a quartz substrate with collective-plasmon modes of a two-dimensional periodic overlayer of gold nanodisks and obtain excellent quantitative agreement with experiment. Moreover, we report a thorough analysis of the optical properties of three-dimensional photonic crystals of metallic nanodisks.

DOI: 10.1103/PhysRevB.77.035101 PACS number(s): 42.70.Qs, 42.25.Bs, 73.20.Mf, 78.67.Bf

I. INTRODUCTION

Metallodielectric nanostructures attract a continuously growing interest because of their fascinating optical properties. These properties are due, to a large extent, to the existence of plasmonic resonances, which can dramatically enhance the local electromagnetic (EM) field by concentrating EM energy into subwavelength volumes, and lead to a plethora of intriguing physical phenomena and applications, such as single molecule Raman scattering,[1] nonlinear optical effects,[2] enhanced random lasing,[3] subwavelength imaging,[4] optical antennas,[5] nanoscale optoelectronic circuits,[6] metamaterials with negative effective permeability at visible frequencies,[7] solar energy absorption,[8] biological sensing,[9] and diagnostic and therapeutic technologies.[10] However, there are often complicating factors in understanding the optical properties of these nanostructures, including the presence of a supporting substrate, a solvent layer, and strong EM coupling between the different building units. All of these factors motivate the need for computationally fast and efficient theoretical methods that can describe the electrodynamics of metallodielectric nanostructures of arbitrary shape and size, subject to a complex external environment.

Among the computational methodologies available for the study of the optical properties of metallodielectric systems containing periodic arrays of particles (scatterers) and homogeneous slabs, the so-called layer-multiple-scattering method has unique advantages.[11–14] Contrary to traditional band-structure or time-domain techniques, this method proceeds at a given frequency, i.e., it is an "on-shell" method and, therefore, it can be directly applied to structures made of strongly dispersive and absorptive materials such as real metals. Besides the complex band structure of a three-dimensional (3D) photonic crystal, associated with a given crystallographic plane, the method allows one to calculate, also, the transmission, reflection, and absorption coefficients of an EM wave incident at a given angle on a finite slab of the crystal and, therefore, it can describe an actual transmission experiment. It is worth noting that periodicity in the direction perpendicular to the layers is not required: the layers must only have the same two-dimensional (2D) periodicity. The layer-multiple-scattering method is proven very efficient for systems of spherical particles. Recently, an extension of the method to the treatment of nonspherical particles, using the extended-boundary-condition approach for the calculation of the single-cell T matrix,[15] was formulated and the applicability of the formalism was demonstrated on a specific example of a photonic crystal of metallic spheroidal particles with a small deviation from the spherical shape.[16]

In the present paper, we employ the above-mentioned extended version of the layer-multiple-scattering method to study photonic systems of 2D and 3D ordered arrays of metallic nanodisks with an aspect ratio as large as 5. Such structures can be synthesized in the laboratory using modern lithographic techniques and attract considerable interest. Systematic investigation of the plasmonic properties of short-range-ordered arrays of noninteracting metallic nanodisks over a large size and spectral range revealed the existence of broad, spectrally tunable particle-plasmon resonances for various metallic materials.[17–19] Moreover, extensive studies of the plasmon resonances in pairs of such nanodisks show a strong redshift of the dipolar resonance for incident polarization parallel to the dimer axis and a small blueshift for polarization perpendicular to this axis, with decreasing interparticle distance.[20–22] On the other hand, systems consisting of 2D periodic arrays of metallic nanodisks on a dielectric layer exhibit unique optical properties such as strong coupling between the particle-plasmon resonance and waveguide modes of the layer[23] and are promising candidates for distributed feedback substrates of organic lasers.[24] It has also been shown that the EM interaction between a 2D grating of resonant metallic nanodisks and a metallic film induces coupled modes of localized particle plasmons and the underlying surface plasmon polariton, which manifest themselves as multiple peaks in the corresponding extinction spectrum.[25] Finally, it is worth noting that, apart from homogeneous metallic nanodisks, more complex disk-shaped nanoparticles, such as hollow disks (nanorings)[26] and alternatively stacked metal-dielectric disks (nanosandwiches),[27,28] also attract considerable attention because they exhibit strong and tunable particle-plasmon resonances.

This paper is organized as follows. In Sec. II, we analyze the optical response of a single metallic nanodisk and discuss the particle-plasmon resonances. In Sec. III, we present nu-

merical results for the transmission and absorption properties of a 2D periodic array of such nanodisks, examine the EM interaction of this array with a homogeneous dielectric waveguiding layer underneath, and compare our results with available experimental data. In Sec. IV, we investigate a 3D photonic crystal of metallic nanodisks; we analyze complex-band-structure diagrams in conjunction with associated transmission spectra of finite slabs of this crystal and demonstrate the physical origin of the field eigenmodes. The last section concludes the paper.

II. SCATTERING BY A SINGLE METALLIC NANODISK

In the present work, we shall be concerned with metallic nanodisks, characterized by a (relative) magnetic permeability $\mu_s=1$ and a (relative) dielectric function ϵ_s, in an otherwise homogeneous dielectric medium. The values of μ and ϵ of the host medium do not play a crucial role; therefore, we choose air as the host material, though other dielectric materials would not alter our conclusions. Moreover, we assume, to begin with, that ϵ_s has the simple yet effective Drude form[29]

$$\epsilon_s(\omega) = 1 - \frac{\omega_p^2}{\omega(\omega + i\tau^{-1})}, \tag{1}$$

where ω_p is the bulk plasma frequency and τ the relaxation time of the conduction-band electrons of the metal, which describes the dissipative losses. When using the Drude dielectric function of Eq. (1), it is convenient to express the frequency in units of ω_p and use c/ω_p as the length unit, where c is the velocity of light in vacuum. We note that, considering a typical value 10 eV for $\hbar\omega_p$, c/ω_p corresponds to about 20 nm.

The scattering properties of a single particle can be obtained through the scattering T matrix. For the numerical evaluation of the elements of the T matrix for the nanodisk, we employ the extended-boundary-condition method,[15] properly adapted.[16] Truncating the relevant angular-momentum expansions at $\ell_{max}=12$, $\ell_{cut}=16$ and using a Gaussian quadrature integration formula with 4000 points for the integrals involved, our results have a relative error less than 10^{-3} in the considered range of frequencies.

The scattering T matrix is defined, in general terms, as the matrix which transforms the incident wave field, of amplitude $\mathbf{a}^0$ into the scattered wave field, of amplitude $\mathbf{a}^+$. In the basis of vector spherical waves, we have

$$a^+_{P\ell m} = \sum_{P'\ell'm'} T_{P\ell m;P'\ell'm'} a^0_{P'\ell'm'}, \tag{2}$$

where $\ell=1,2,\ldots$ and $m=-\ell,-\ell+1,\ldots,\ell$ are the usual angular-momentum indices and $P=E,H$ denotes the electric and magnetic multipole modes, respectively. For a spherical scatterer, $T_{P\ell m;P'\ell'm'}=T_{P\ell}\delta_{PP'}\delta_{\ell\ell'}\delta_{mm'}$. The causality condition implies that the eigenvalues of the T matrix are analytic functions in the upper complex frequency half-plane but they may have poles in the lower half-plane at $\omega_i - i\gamma_i$, $\gamma_i \geq 0$; ω_i is the eigenfrequency, while γ_i denotes the inverse of the lifetime of the respective mode. Among all possible solutions, resonant modes with $\gamma_i/\omega_i \ll 1$ are of particular physical interest. For example, a metallic nanosphere in a dielectric host medium exhibits such 2^ℓ-pole resonant modes of electric type at $\omega_\ell \simeq \omega_p\sqrt{\ell/[\ell+(\ell+1)\epsilon]}$. These correspond to collective electron oscillations at the surface of the particle and are termed particle-plasmon modes. Similar plasmon modes also subsist in nonspherical particles but, in this case, $T_{P\ell m;P'\ell'm'}$ is no longer a diagonal matrix and thus there is no clear characterization of multipole modes. Nevertheless, the cylindrical symmetry of the disk implies a block-diagonal form for the corresponding T matrix, and its eigenvalues are characterized by a given value of $|m|$ and a given parity, i.e., the corresponding eigenfields are either even or odd upon inversion. In terms of group theory, we can say that, since a disk is invariant under the symmetry operations of the $D_{\infty h}$ group, its eigenmodes belong to the irreducible representations of this group.[30]

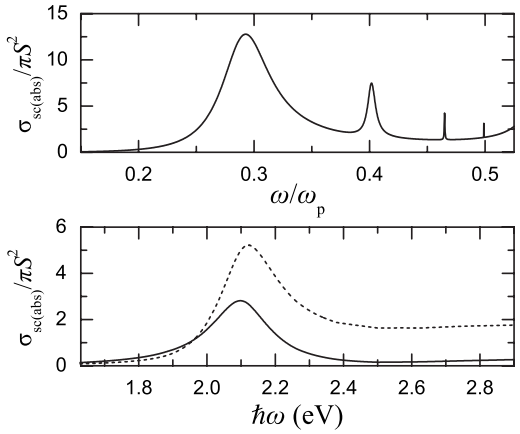

FIG. 1. The scattering (solid lines) and absorption (dashed lines) cross sections of a gold nanodisk in air, for p-polarized light incident at an angle 45° with respect to the disk axis. Upper diagram: the disk has a diameter $d\equiv 2S=5c/\omega_p$ and a thickness $h=c/\omega_p$; its dielectric function is given by Eq. (1) with $\tau^{-1}=0$, which implies that the absorption cross section is identically zero. Lower diagram: the experimental dielectric function of bulk gold (Ref. 31) is used for a disk of dimensions $d=100$ nm and $h=20$ nm.

In the upper diagram of Fig. 1, we show the scattering cross section, normalized to the geometric cross section, for a single metallic nanodisk in air. The disk is described by the Drude dielectric function given by Eq. (1) without dissipative losses ($\tau^{-1}=0$) and has a diameter $d\equiv 2S=5c/\omega_p$ and a thickness $h=c/\omega_p$. In this case, obviously, the absorption cross section vanishes. An incoming plane wave is incident at an angle $\theta=45°$ with respect to the disk axis (taken as the z axis) and is p polarized, i.e., the electric field oscillates in the plane of incidence, which is defined by the disk axis and the direction of incidence. The excitation of several particle-plasmon modes is clearly visible in the figure. The peaks at $0.293\omega_p$, $0.402\omega_p$, and $0.465\omega_p$ are associated with particle-plasmon modes corresponding to $m=\pm 1$, $m=\pm 2$, and $m=\pm 3$, respectively. Higher order modes, e.g., that at $0.499\omega_p (m=\pm 4)$, are hardly discernible in the figure. All these modes are predominantly of electric type and have a mainly dipole, quadrupole, octapole, etc., character, respec-

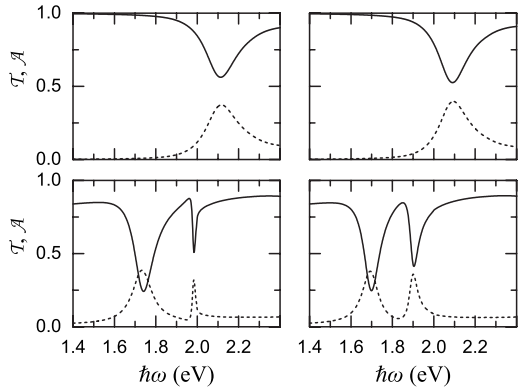

FIG. 2. Upper panel: transmittance (solid lines) and absorbance (dashed lines) of a rectangular array (a_{0x}=425 nm, a_{0y}=300 nm) of gold nanodisks (d=100 nm, h=20 nm) for x-polarized (left-hand diagram) and y-polarized (right-hand diagram), normally incident light. The lower panel shows the corresponding diagrams if the array of nanodisks is placed on top of an ITO film, of thickness 140 nm, on a quartz substrate.

tively. In terms of group theory, their symmetries are E_{1u}, E_{2g}, E_{3u}, etc.[30]

In the lower diagram of Fig. 1, we show the normalized scattering and absorption cross sections of an actual gold nanodisk, of dimensions d=100 nm and h=20 nm, in air. Here, for the dielectric function of gold, we interpolate to the bulk values measured by Johnson and Christy[31] that include dissipative losses. It can be seen from the figure that, in the frequency region which interests us here, only the lowest E_{1u} resonance survives. The higher particle-plasmon modes are fully absorbed: they do not manifest themselves in the scattering cross section and appear as a broad background in the absorption cross section. This happens, obviously, because these modes have very long lifetimes as compared to the absorption time.

III. STRUCTURES OF TWO-DIMENSIONAL ARRAYS OF METALLIC NANODISKS

Let us assume, to begin with, a 2D rectangular lattice defined by the primitive vectors $\mathbf{a}_1=(a_{0x},0,0)$ and $\mathbf{a}_2=(0,a_{0y},0)$, with lattice constants a_{0x}=425 nm and a_{0y}=300 nm, of gold nanodisks (d=100 nm, h=20 nm) in air. For the given system, using the same cutoff parameters as for the single nanodisk, we obtain very good convergence in the numerical calculations. Because of the 2D periodicity of the structure under consideration, the xy component of the wave vector $\mathbf{q}=(\mathbf{q}_\parallel,q_z)$ of an incident wave, reduced within the surface Brillouin zone (BZ), $\mathbf{k}_\parallel$, is a conserved quantity in the scattering process. In the upper panel of Fig. 2, we show the transmittance and absorbance of the system at normal incidence, i.e., for $\mathbf{q}_\parallel=\mathbf{k}_\parallel=\mathbf{0}$, in the frequency region of the lowest particle-plasmon modes. The calculations were carried out using the experimental dielectric function of bulk gold.[31] For $\mathbf{k}_\parallel=\mathbf{0}$, the eigenmodes of the system have the symmetry of the irreducible representations of the D_{2h} group $(N_1,N_2,N_3,N_4,N_{1'},N_{2'},N_{3'},N_{4'})$ and the doubly degenerate E_{1u} particle-plasmon modes, which are relevant here, give an $N_{1'}$ and an $N_{4'}$ mode.[30] On the other hand, a plane EM wave propagating in the host region normal to the given layer projects onto the N_3 and $N_{1'}$ or the N_2 and $N_{4'}$ representations if it is polarized along x or y, respectively, and excites modes of the plane of nanodisks of the appropriate symmetry (see upper panel of Fig. 2). The doubly degenerate lowest E_{1u} plasmon mode of the single nanodisk at 2.098 eV splits, for $\mathbf{k}_\parallel=\mathbf{0}$, into two collective-plasmon states: one of $N_{1'}$ symmetry at 2.113 eV and one of $N_{4'}$ symmetry at 2.091 eV. In general, the above plasmon modes of the individual particles interact weakly between them and form two relatively narrow bands, $\omega(\mathbf{k}_\parallel)$, about the corresponding eigenfrequency of the single particle. These bands have the symmetry of the irreducible representations of the point group that leaves $\mathbf{k}_\parallel$ invariant. For example, for $\mathbf{k}_\parallel=(k_x,0)$, the appropriate point group is C_{1h}. This group has two irreducible representations, Q_1 and Q_2, with basis functions which are even (Q_1) and odd (Q_2) upon reflection with respect to the xz plane, and the E_{1u} particle-plasmon modes that interest us here give a Q_1 and a Q_2 band. We note that a plane EM wave propagating in the host medium with a $\mathbf{k}_\parallel$ along the x direction has the Q_1 or Q_2 symmetry if it is p or s polarized, respectively, i.e., if the electric field oscillates in or normal to the plane of incidence (the xz plane). An $N_{1'}$ or an $N_{4'}$ mode for $\mathbf{k}_\parallel=\mathbf{0}$ now becomes a mode of Q_1 or Q_2 symmetry which is excited by a p- or s-polarized incident wave, respectively.

If the above rectangular array of nanodisks is placed on top of a dielectric film, interesting effects can take place.[23] The uncoated dielectric film, sandwiched between two semi-infinite media with refractive indices smaller than that of the film, supports, besides the scattering states, also waveguide modes. Along any direction parallel to the interfaces, these modes have the form of propagating waves with a wave vector $\mathbf{q}_\parallel$; along the normal direction, they decay exponentially to zero away from the film on either side of it. There are transverse electric (TE) guided modes (the electric field oscillates parallel to the interfaces) and transverse magnetic (TM) guided modes (the magnetic field oscillates parallel to the interfaces). These modes lie outside the light cone in the surrounding media and, therefore, cannot be excited by an externally incident wave. They cannot match continuously a propagating mode of the EM field outside the film; momentum and energy cannot be conserved simultaneously. The presence of a 2D periodic array of particles on the film transforms waveguide modes from bound to radiative through an umklapp process: a plane wave of wave number q, incident on the periodic array, generates a number of diffracted beams with wave vectors $\mathbf{K}_\mathbf{g}^\pm=\mathbf{k}_\parallel+\mathbf{g}\pm\sqrt{q^2-(\mathbf{k}_\parallel+\mathbf{g})^2}\hat{\mathbf{z}}$, where $\mathbf{g}$ are 2D reciprocal-lattice vectors. If $q<|\mathbf{k}_\parallel+\mathbf{g}|$, we obtain evanescent diffracted beams which can match continuously the corresponding guided waves of the same polarization and of the same $\mathbf{q}_\parallel=\mathbf{k}_\parallel+\mathbf{g}$, provided they have the right frequency. Accordingly, the waveguide modes are no longer bound within the film but leak into the outer region becoming resonant states. These modes can be excited by an externally incident wave and manifest themselves as resonance structures in the transmission spectrum. From another point of view, because of the 2D periodicity of the coating layer, the

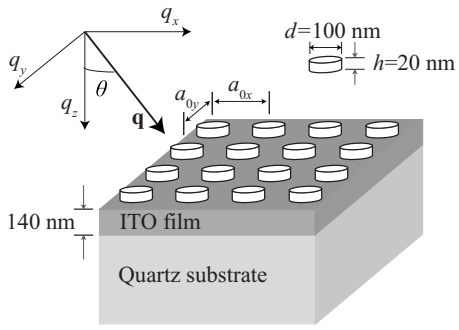

FIG. 3. Schematic view of a rectangular array of gold nanodisks on top of an ITO film, on a quartz substrate.

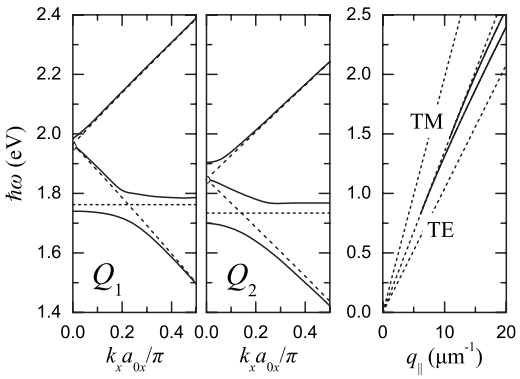

FIG. 4. Left-hand panel: dispersion curves of the Q_1 and Q_2 resonant states, associated with $\mathbf{k}_\parallel=(k_x,0)$, of a rectangular array (a_{0x}=425 nm, a_{0y}=300 nm) of gold nanodisks (d=100 nm, h=20 nm) on top of an ITO film, of thickness 140 nm, on a quartz substrate. The open semicircles at $\mathbf{k}_\parallel=\mathbf{0}$ denote the optically inactive modes. The dashed lines show, separately, the corresponding dispersion curves of the waveguide modes in the reduced-zone scheme and of the particle-plasmon modes (schematically drown as horizontal lines), in the absence of interaction between them. It is worth noting that, away from the frequency region of the particle-plasmon modes, the dispersion lines of the waveguide modes are practically unaffected by the existence of the gold nanodisk array. Right-hand panel: dispersion curves of the TE and TM waveguide modes for an ITO film, of thickness 140 nm, sandwiched between air and quartz. The dashed lines define the light cone in air ($\omega=cq_\parallel$), quartz ($\omega=cq_\parallel/\sqrt{\epsilon_q\mu_q}$), and ITO ($\omega=cq_\parallel/\sqrt{\epsilon_{\mathrm{ITO}}\mu_{\mathrm{ITO}}}$).

waveguide frequency bands are folded within the surface BZ of the given lattice and acquire a small imaginary part due to the mixing with the extended (scattering) states.

Let us consider the above 2D array of nanodisks on top of an indium tin oxide (ITO) film ($\epsilon_{\mathrm{ITO}}=3.6, \mu_{\mathrm{ITO}}=1$), 140 nm thick, on a quartz substrate ($\epsilon_q=2.13, \mu_q=1$), as shown in Fig. 3. This film supports waveguide modes in the frequency region of interest. Because of the absence of horizontal plane of mirror symmetry in the composite structure, the appropriate point group is C_{2v} instead of D_{2h} and the eigenmodes of the system for $\mathbf{k}_\parallel=\mathbf{0}$ are classified according to the irreducible representations Z_1, Z_2, Z_3, and Z_4 of C_{2v}.[30] In this respect, the N_1, and N_4, particle-plasmon modes of the plane of nanodisks now have the Z_3 and Z_4 symmetries, respectively. In the lower panel of Fig. 2, we show the transmittance and absorbance of the system at normal incidence and polarization along x and y. The resonances at 1.741 and 1.699 eV arise from the excitation of the Z_3 and Z_4 particle-plasmon modes of the plane of nanodisks, respectively. Comparing with the results shown in the upper panel of Fig. 2, it can be seen that the presence of the film and the substrate induces a considerable redshift of the particle-plasmon modes. In addition, we observe two relatively sharp resonance structures which originate from appropriate waveguide modes. The one, at 1.984 eV, corresponds to a TM mode and is excited by an x-polarized incident wave (it has the Z_3 symmetry); the other, at 1.904 eV, corresponds to a TE mode and is excited by a y-polarized incident wave (it has the Z_4 symmetry). In order to ensure adequate convergence, here, we need to truncate the angular-momentum expansions at $\ell_{\max}=12$ and take into account 161 $\mathbf{g}$ vectors in the relevant plane-wave expansions, while the T matrix is calculated with $\ell_{\mathrm{cut}}=16$ and a Gaussian quadrature integration formula with 4000 points.[16]

By varying the direction of incidence, we can deduce the dispersion diagram of the resonant modes of the composite system. The results for $\mathbf{k}_\parallel=(k_x,0)$ are depicted in the left-hand panel of Fig. 4. There, we show, in addition, by the dashed lines, the bands of waveguide and collective particle-plasmon modes in the absence of interaction between them. Along this direction, the appropriate point group is, again, C_{1h}. It can be seen that states of the same symmetry interact and repel each other, giving rise to a band diagram of hybridized waveguide and particle-plasmon modes. The same mechanism removes, also, the degeneracy of the waveguide states at the edges and the center of the surface BZ, giving rise to small Bragg gaps. In the frequency region under consideration, there are two such gaps at $\mathbf{k}_\parallel=\mathbf{0}$. For the Q_1 modes, the state below the Bragg gap has the Z_1 symmetry, and that above the gap the Z_3 symmetry. For the Q_2 modes, the state below the Bragg gap has the Z_2 symmetry, and that above the gap the Z_4 symmetry. We note again that Z_3 or Z_4 states can be excited by a normally incident wave polarized along x or y, respectively, while Z_1 or Z_2 states are optically inactive in our case and do not manifest themselves in the corresponding transmission and absorption spectra. In the right-hand panel of Fig. 4, we show the dispersion diagram of the waveguide modes of the ITO film on a quartz substrate without the coating layer of nanodisks.

We shall now compare our results with available experimental data for different rectangular arrays of gold nanodisks (d=100 nm, h=20 nm) on top of an ITO film, 140 nm thick, on a quartz substrate.[23] We first study the optical response of a structure with a_{0x}=425 nm and a_{0y}=300 nm, for light incident at an angle in the xz plane and polarization along the y direction (s polarization). In this case, two Q_2 waveguide modes and one Q_2 particle-plasmon mode (see Fig. 4) are excited. Figure 5 depicts the relative extinction (extinction =negative logarithm of the transmittance) of the system with respect to the uncoated ITO film on the quartz substrate, i.e., the quantity $-\ln(\mathcal{T}/\mathcal{T}_0)$, where $\mathcal{T}$ ($\mathcal{T}_0$) is the transmittance of the quartz-ITO-air system with (without) the coating layer of nanodisks, for different angles of incidence. In order to obtain good quantitative agreement between experiment and theory as far as the peak positions are concerned, we shift the

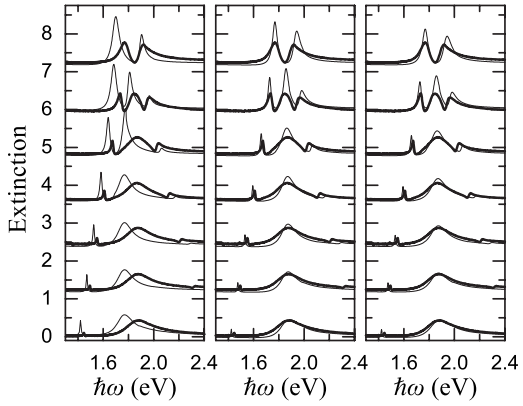

FIG. 5. Experimental (Ref. 23) (thick lines) and theoretical (thin lines) extinction spectra of a rectangular array (a_{0x}=425 nm, a_{0y}=300 nm) of gold nanodisks (d=100 nm, h=20 nm) on top of an ITO film, 140 nm thick, on a quartz substrate, for incidence in the xz plane at an angle θ and polarization along the y direction. The different spectra are shifted upward for clarity and correspond, from top to bottom, to θ varying from 0° to 30° with a step of 5°. Left-hand panel: nanodisks without finite-size correction, placed on the ITO film. Middle panel: nanodisks without finite-size correction, placed 3 nm above the ITO film. Right-hand panel: nanodisks with finite-size correction, placed 3 nm above the ITO film.

nanodisk array by 3 nm away from the ITO film (see middle panel of Fig. 5). We note that a small separation of the nanodisks from the ITO film may also exist in the lithographically fabricated samples, e.g., due to the presence of a buffer layer. A general observation is that particle-plasmon resonances appear sharper in the theoretical than in the experimental spectra. This is likely to be ascribed to finite-size effects in the optical response of the nanodisks as well as to fabrication imperfections in particle shape, size, and arrangement. In the case of a small metallic particle, the electronic mean free path is shorter than in the bulk metal and this effect can be incorporated by adding a size-dependent correction $\Delta\epsilon = \omega_p^2[(\omega^2+i\omega\tau^{-1})^{-1}-(\omega^2+i\omega\tau_s^{-1})^{-1}]$ to the bulk dielectric function, where $\tau_s^{-1}=\tau^{-1}+v_F L^{-1}$ is the inverse relaxation time corrected for the finite size of the particle, v_F is the Fermi velocity in the bulk material, and L is an appropriate linear dimension of the particle.[32] The results obtained if we take into account this finite-size correction using the values $\hbar\omega_p$=9 eV, $\hbar\tau^{-1}$=0.06 eV, and $\hbar v_F$=0.9 eV nm which are appropriate for gold[29,31] and L=30 nm as a typical linear dimension of the nanodisk[32] show, indeed, a broadening of the peaks, in better agreement with the experiment, as can be seen in the right-hand panel of Fig. 5.

Figure 6 depicts theoretical and experimental results for corresponding extinction spectra of different rectangular arrays of gold nanodisks on top of the ITO film on a quartz substrate, at normal incidence and polarization along the y direction. It can be seen that there is excellent agreement between experiment and theory. By increasing the lattice constant a_{0x}, the surface BZ shrinks and the waveguide modes at the center of the surface BZ that are excited are shifted to lower frequencies. In this way, one can change the position of the waveguide modes relatively to that of the particle-plasmon modes (and therefore their interaction) in a controllable manner, as shown in Fig. 6.

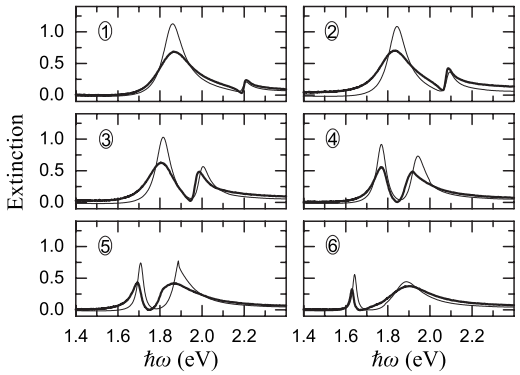

FIG. 6. Experimental (Ref. 23) (thick lines) and theoretical (thin lines) extinction spectra of rectangular arrays of gold nanodisks (d=100 nm, h=20 nm) placed 3 nm above an ITO film, 140 nm thick, on a quartz substrate, at normal incidence and polarization along the y direction. The sequential diagrams correspond to a_{0x} varying from 350 to 475 nm with a step of 25 nm, and a_{0y}=300 nm.

IV. PHOTONIC CRYSTAL OF METALLIC NANODISKS

As an example of a 3D structure, we consider a simple cubic (sc) crystal, with lattice constant $a=10c/\omega_p$, of metallic nanodisks described by the Drude dielectric function, with dimensions $d=5c/\omega_p$ and $h=c/\omega_p$, in air, and view the crystal as a sequence of (001) planes of particles. We deliberately disregard absorption in the metallic material, taking $\tau^{-1}=0$ in Eq. (1), in order to be able to calculate the frequency band structure in an unambiguous manner. In the numerical calculations, we consider $\ell_{\max}=10$ and 37 **g** vectors, while the T matrix is evaluated with $\ell_{\text{cut}}=14$ and 2000 points for the Gaussian integration, in order to ensure adequate convergence. In the left-hand panel of Fig. 7, we

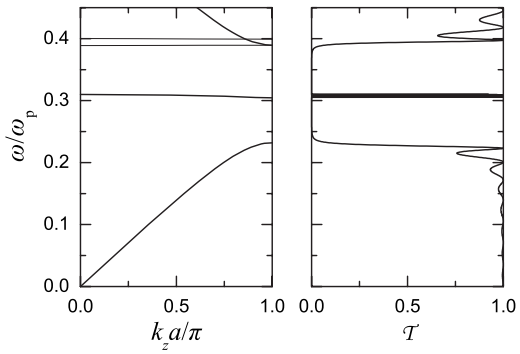

FIG. 7. Left-hand diagram: the photonic band structure of a sc photonic crystal, with lattice constant $a=10c/\omega_p$, of nanodisks ($d=5c/\omega_p$, $h=c/\omega_p$) made of a nonabsorbing Drude metal, in air, along the [001] direction. The thick and thin lines show the doubly degenerate and nondegenerate bands, respectively. Right-hand diagram: transmittance at normal incidence of a slab of eight (001) planes of the above crystal.

show the photonic band structure of this crystal along the [001] direction, i.e., for $\mathbf{k}_{\parallel}=\mathbf{0}$. The symmetry of the bands along this direction is that of the C_{4v} group: Δ_1, Δ_2, $\Delta_{1'}$, $\Delta_{2'}$, and Δ_5.[30] The bands Δ_1, Δ_2, $\Delta_{1'}$, and $\Delta_{2'}$ are nondegenerate and Δ_5 is doubly degenerate. We note that the (001) surface of the crystal under consideration is a plane of mirror symmetry and, therefore, the frequency bands appear in pairs: $k_z(\omega,\mathbf{k}_{\parallel})$ and $-k_z(\omega,\mathbf{k}_{\parallel})$. For this reason, in Fig. 7, we show the bands only for positive k_z.

In the long wavelength limit, we obtain a linear dispersion curve, of Δ_5 symmetry, as expected for propagation in a homogeneous effective medium. This extended effective-medium band is folded within the first BZ and a relatively wide Bragg gap opens up at the BZ boundary. In addition, flatbands are formed from the particle-plasmon modes of the individual nanodisks that interact weakly between them. Along the [001] direction, in the frequency region under consideration, there is one doubly degenerate flatband of Δ_5 symmetry within the gap, which originates from the lowest E_{1u} particle-plasmon modes. Moreover, the lowest E_{2g} particle-plasmon modes give rise to one $\Delta_{2'}$ and one Δ_2 flatband, about $0.39\omega_p$ and $0.40\omega_p$, respectively. We note that the eigenmodes of the EM field at the center $[\mathbf{k}=(0,0,0)]$ and the boundary $\mathbf{k}=(0,0,\pi/a)$ of the first BZ have the symmetry of the D_{4h} group. Since none of the irreducible representations of this group is three dimensional, the threefold degeneracy which appears at $0.389\omega_p$ at the BZ boundary is accidental and is removed if we change, e.g., the lattice constant of the given crystal.

The right-hand panel of Fig. 7 shows the transmittance of a slab of the crystal under consideration consisting of eight (001) planes of nanodisks. The transmittance opposite the extended effective-medium band is about unity and exhibits the well-known Fabry-Pérot oscillations due to multiple scattering between the surfaces of the slab; the period of these oscillations corresponds to $k_z a/\pi=1/8$, as expected for the given slab thickness. Within the gap region, the transmission coefficient practically vanishes, except in the short frequency range of the Δ_5 flatband where resonant transmission takes place.

The right-hand panel of Fig. 8 displays the photonic band structure of the given crystal in more detail, over a limited frequency region about the lowest E_{1u} and E_{2g} particle-plasmon modes, for $\mathbf{k}_{\parallel}=(0.3\pi/a,0)$. Apart from the ordinary frequency bands (k_z is real), we show, over the gap regions, the real-frequency lines with the smallest imaginary part of k_z. For $\mathbf{k}_{\parallel}=(k_x,0)$, $0<k_x<\pi/a$, the point group of the wave vector is the C_{1h} group. Therefore, according to group theory, a doubly degenerate band of Δ_5 symmetry (for $\mathbf{k}_{\parallel}=\mathbf{0}$) splits for $\mathbf{k}_{\parallel}=(k_x,0)$ into one band of Q_1 and one of Q_2 symmetry; similarly, a $\Delta_{2'}$ or Δ_2 band gives a Q_2 or Q_1 band, respectively, as shown in the right-hand panel of Fig. 8. An s- or p-polarized EM wave incident on a finite (001) slab of the crystal with $\mathbf{k}_{\parallel}=(k_x,0)$ excites bands of Q_2 or Q_1 symmetry, respectively, and through them is transmitted to the other side of the slab. In the regions of frequency gaps, where there are no propagating Bloch modes, the transmission coefficient is determined from the complex band of the proper symmetry which has the smallest imaginary part: the wave

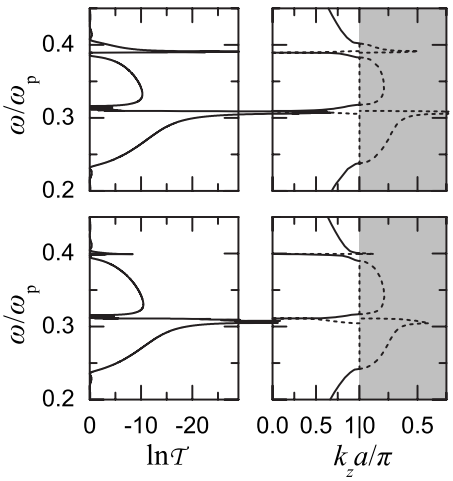

FIG. 8. Left-hand panel: transmission coefficient of an s-polarized (upper diagram) and a p-polarized (lower diagram) wave incident on a slab of eight (001) planes of the photonic crystal of Fig. 7 with $\mathbf{q}_{\parallel}=(0.3\pi/a,0)$. Right-hand panel: the corresponding complex band structure for the Q_2 (upper diagram) and the Q_1 (lower diagram) bands. In the gap regions, we show by dashed lines the real-frequency lines with the smallest imaginary part of k_z (plotted in the shaded area).

decreases exponentially within the slab with an attenuation coefficient equal to $\mathrm{Im}\,k_z(\omega)$ of this band, as shown in the left-hand panel of Fig. 8.

V. CONCLUSIONS

In summary, we employed the extended layer-multiple-scattering method to study the optical response of plasmonic systems of 2D and 3D ordered arrays of metallic nanodisks and showed that the method retains its high efficiency and accuracy even in cases of particles with edges and strong deviation from the spherical shape. Starting from a detailed analysis of the particle-plasmon modes of a single metallic nanodisk, we studied the interaction between waveguide modes of an ITO film on a quartz substrate and collective plasmonic modes of 2D periodic overlayers of gold nanodisks. Our results are in very good quantitative agreement with available experimental data, thus demonstrating that the layer-multiple-scattering method is a valuable tool for the study of layered plasmonic nanostructures of particles of arbitrary shape. Finally, we investigated a 3D photonic crystal of metallic nanodisks; we provided a consistent interpretation of transmission spectra of finite slabs of this crystal by reference to relevant complex-band-structure diagrams and demonstrated the physical origin of the field eigenmodes.

ACKNOWLEDGMENTS

This work was supported by the research program "Kapodistrias" of the University of Athens. We are grateful to A. Christ and co-workers[23] for providing us with their experimental data.

[1] S. M. Nie and S. R. Emory, Science **275**, 1102 (1997).
[2] M. D. McMahon, R. Lopez, R. F. Haglund, E. A. Ray, and P. H. Bunton, Phys. Rev. B **73**, 041401(R) (2006).
[3] O. Popov, A. Zilbershtein, and D. Davidov, Appl. Phys. Lett. **89**, 191116 (2006).
[4] A. Ono, J.-I. Kato, and S. Kawata, Phys. Rev. Lett. **95**, 267407 (2005).
[5] P. Muhlschlegel, H. J. Eisler, O. J. F. Martin, B. Hecht, and D. W. Pohl, Science **308**, 1607 (2005).
[6] E. Ozbay, Science **311**, 189 (2006).
[7] A. N. Grigorenko, A. K. Geim, H. F. Gleeson, Y. Zhang, A. A. Firsov, I. Y. Khrushchev, and J. Petrovic, Nature (London) **438**, 17 (2005).
[8] J. R. Cole and N. J. Halas, Appl. Phys. Lett. **89**, 153120 (2006).
[9] A. P. Alivisatos, Nat. Biotechnol. **22**, 47 (2004).
[10] A. M. Gobin, M. H. Lee, N. J. Halas, W. D. James, R. A. Drezek, and J. L. West, Nano Lett. **7**, 1929 (2007).
[11] N. Stefanou and A. Modinos, J. Phys.: Condens. Matter **3**, 8135 (1991).
[12] N. Stefanou, V. Yannopapas, and A. Modinos, Comput. Phys. Commun. **113**, 49 (1998).
[13] N. Stefanou, V. Yannopapas, and A. Modinos, Comput. Phys. Commun. **132**, 189 (2000).
[14] A. Modinos, N. Stefanou, and V. Yannopapas, Opt. Express **8**, 197 (2001).
[15] M. I. Mishchenko, L. D. Travis, and A. A. Lacis, *Scattering, Absorption, and Emission of Light by Small Particles* (Cambridge University Press, Cambridge, 2002).
[16] G. Gantzounis and N. Stefanou, Phys. Rev. B **73**, 035115 (2006).
[17] P. Hanarp, M. Käll, and D. S. Sutherland, J. Phys. Chem. B **107**, 5768 (2003).
[18] C. Langhammer, Z. Yuan, I. Zorić, and B. Kasemo, Nano Lett. **6**, 833 (2006).
[19] C. Langhammer, B. Kasemo, and I. Zorić, J. Chem. Phys. **126**, 194702 (2007).
[20] T. Atay, J.-H. Song, and A. V. Nurmikko, Nano Lett. **4**, 1627 (2004).
[21] L. Gunnarsson, T. Rindzevicius, J. Prikulis, B. Kasemo, M. Käll, S. Zou, and G. C. Schatz, J. Phys. Chem. B **109**, 1079 (2005).
[22] P. K. Jain, W. Huang, and M. A. El-Sayed, Nano Lett. **7**, 2080 (2007).
[23] A. Christ, S. Linden, T. Zentgraf, D. Nau, S. G. Tikhodeev, N. A. Gippius, J. Kuhl, F. Schindler, A. W. Holleitner, J. Stehr, J. Crewett, J. Lupton, T. Klar, U. Scherf, J. Feldmann, C. Dahmen, G. von Plessen, and H. Giessen, in *Photonic Crystals: Advances in Design, Fabrication, and Characterization*, edited by K. Busch, S. Lölkes, R. B. Wehrspohn, and H. Föll (Wiley, New York, 2004), p 85.
[24] J. Stehr, J. Crewett, F. Schindler, R. Sperling, G. von Plessen, U. Lemmer, J. M. Lupton, T. A. Klar, J. Feldmann, A. W. Holleitner, M. Forster, and U. Scherf, Adv. Mater. (Weinheim, Ger.) **15**, 1726 (2003).
[25] J. Cesario, R. Quidant, G. Badenes, and S. Enoch, Opt. Lett. **30**, 3404 (2005).
[26] J. Aizpurua, P. Hanarp, D. S. Sutherland, M. Käll, G. W. Bryant, and F. J. García de Abajo, Phys. Rev. Lett. **90**, 057401 (2003).
[27] K. H. Sy, Q. H. Wei, and X. Zhang, Appl. Phys. Lett. **88**, 063118 (2006).
[28] A. Dmitriev, T. Pakizeh, M. Käll, and D. S. Sutherland, Small **3**, 294 (2007).
[29] N. W. Ashcroft and N. D. Mermin, *Solid State Physics* (Saunders, New York, 1976).
[30] J. F. Cornwell, *Group Theory in Physics* (Academic, London, 1984), Vol. 1.
[31] P. B. Johnson and R. W. Christy, Phys. Rev. B **6**, 4370 (1972).
[32] W. A. Kraus and G. C. Schatz, J. Chem. Phys. **79**, 6130 (1983).